Environmental Science and Pollution Research (2018) 25:23973–23985
https://doi.org/10.1007/s11356-018-2433-0

RESEARCH ARTICLE

# Water content of limestones submitted to realistic wet deposition: a CIME2 chamber simulation

Anne Chabas[1] · Jean-Pierre Sizun[2] · Lucile Gentaz[1] · Pauline Uring[1] · Alain Phan[1] · Adriana Coman[1] · Stéphane Christophe Alfaro[1] · Mandana Saheb[1] · Edouard Pangui[1] · Pascal Zapf[1] · Florian Huet[3]

Received: 15 February 2018 / Accepted: 28 May 2018 / Published online: 8 June 2018


## Abstract

An experimental chamber (CIME2) has been specially designed to simulate wet atmospheric deposition on limestones used in Paris cultural heritage. This instrument is a complementary tool to CIME, a previously developed chamber dedicated to the simulation of dry atmospheric deposition on monuments and artifacts. The aim of this paper is to describe CIME2 and characterize the wet deposits produced inside it. Mist (fog), drizzle, and rainfall are differentiated in order to document their ability to saturate the limestones most currently used in Paris monuments: The Saint-Maximin's limestone, the Liais of Saint-Maximin, and the Chauvigny's limestone are tested. The comparison between normalized and environmental petrophysical data shows that in the wet deposition simulations, limestones are not systematically water-saturated. Moreover, the realistic experimental conditions chosen favor a more rapid evaporation of the stone water. The quantification of the non-saturation state is a first step that has to be taken into account to improve the geochemical models used to predict the alteration.

**Keywords** Mist · Drizzle · Rain · Capillary imbibition · Evaporation · Adsorption · Limestone · Paris · Saturation · Unsaturation

## Introduction

Among the various weathering factors affecting the cultural heritage materials, water plays a prominent role. In vapor or liquid phase, water is involved in immission processes such as dry and wet atmospheric deposition, respectively. For carbonate stones, the reviews of Livingston (1992), Smith and Viles (2006), and Livingston (2016) identified three main water-dependent weathering mechanisms: dry deposition, karst effect, and acid rain.

Dry deposition is the result of reactions involving gaseous pollutants such as $SO_2$, $NO_2$, particulate matter, water vapor, and the carbonate (i.e., limestone, marble, travertine…) substrate. Indeed, water vapor favors the reactivity of gaseous pollutants with the stone's surface, leading to an enrichment in sulfur or nitrogen of the deposits appearing on the surface and in the subsurface of the stone. Dry deposition was recognized as the main factor responsible for the development of gypseous black crusts in the parts of the monuments not directly exposed to the rain (Sabbioni 2003; Bonazza and Sabbioni 2016). Moreover, even in absence of pollutant, a relative humidity (RH) higher than 75% enhances the adsorption of water on the surface and capillary condensation in the subsurface of minerals (Fripiat et al. 1971) and stone materials (Rousset 2001). In the case of fog or mist event associated with larger (> 95%) RH, a surface condensation occurs on materials whose surface in colder than the air (Camuffo 2016).

**Highlights** • An experimental chamber designed for studying wet deposition on cultural heritage materials is described and characterized.
• Petrophysical measurements are performed in simulated Parisian environment.
• Rainfall, drizzle, and mist deposits are differentiated to evaluate their ability to saturate different porous networks.

Responsible editor: Michel Sablier

✉ Anne Chabas
anne.chabas@lisa.u-pec.fr

[1] Laboratoire Interuniversitaire des Systèmes Atmosphériques, LISA, UMR CNRS 7583, Université Paris Est Créteil et Université Paris Diderot, Institut Pierre Simon Laplace, 61, av du Général de Gaulle, 94010 Créteil Cedex, France

[2] Laboratoire Chrono-environnement UMR6249, CNRS-Université de Bourgogne-Franche-Comté, 16 Route de Gray, 25000 Besançon, France

[3] OSU-Efluve, Université Paris Est Créteil Val de Marne, 61, av du Général de Gaulle, 94010 Créteil Cedex, France

Conversely, the karst effect and acid rain processes belong to the "wet deposition" category. Due to their large surface tension, droplets run off along the building surface and carry away the elements dissolved from the material. This leads to a loss of matter that can be quantified in terms of surface recession rate, surface lowering, or erosion (Inkpen et al. 2012; Steiger 2016). The karstification or karst effect corresponds to limestone dissolution and leaching by rain water droplets having a pH between 5 and 7 because they are in equilibrium with the usual $CO_2$ atmospheric concentrations. Karstification is a phenomenon known to have been active over geological time-scales (Plummer and Wigley 1976; Buhmann and Dreybrodt 1985). At the shorter historical time-scales relevant for the study of the alteration of calcareous monuments, dissolution features and microkarstification are also observable on the areas of the object or structure well exposed to the water runoff (Icomos 2008). Acid rain phenomenon has been documented since the nineteenth century and its transboundary effects have been demonstrated in the late 1960s (Le Moullec and Mezdour 2011). Acid rains have a pH lower than 5.6, because of the additional dissolution of gaseous pollutants such as $SO_2$, $NO_2$, and $NH_3$ in the rain droplets. This low pH makes it particularly active on limestone monuments as it enhances dissolution of the substrate. Therefore, acid rain has been considered for a long time as being the main wet deposition alteration factor. However, it was recently shown that because of the progressive decline of atmospheric acidic pollutants, the karst effect will become the dominant alteration factor in the next future (Bonazza et al. 2009). This is confirmed by the recent decreasing impact of air pollution on the Paris limestone (Lefèvre et al. 2016) and a recent analysis of the Paris rains showing that their mean and median pH are 6.1 and 6.5, respectively (Beysens et al. 2017).

Laboratory tests in corrosion chamber are the go-to methodology to ensure an accelerated degradation of materials. Two different—more or less drastic—approaches can be used:

- The first one consists in increasing dramatically the aggressiveness of the environment in the chambers. This can be done either by replacing of the gaseous by liquid acid attacks (Dewanckele et al. 2014) or by increasing the pollutant concentrations by several orders of magnitude (e.g., from ppb to ppm) (Tétreault et al. 2013);
- The second approach consists in simulating more realistic environmental conditions (Ausset et al. 1996). This approach was chosen to document and understand the initial stages of the microstructural alteration of carbonate rocks by dry atmospheric deposition (Unterwurzacher and Mirwald 2008; Franzoni and Sassoni 2011) or to study the specific impacts of runoff and stagnant water on bronzes (Bernardi et al. 2009; Chiavari et al. 2010). The CIME chamber (Chabas et al. 2015) was designed and characterized adopting this second approach. To complete the dry atmospheric deposition (gas + particles) simulations of CIME, the CIME2 chamber was developed to allow reproducing wet atmospheric deposition.

The aim of this paper is to provide an in-depth characterization of CIME2 and of the precipitations that can be reproduced in it: (1) classical precipitations such as rain and drizzle and (2) "occult" precipitations (mist). The tests are performed on three limestones used in Paris monuments. These limestones are first studied by a normative petrophysical characterization then by simulation of rain, drizzle, and mist. The final objective is to quantify the saturation or unsaturation levels of these limestones when submitted to realistic rain, drizzle, or mist events, considering that they are in façade, which means that they are not subject to the action of capillary rise from the ground.

## Materials and methods

### Sample origins

Stones representative of the Parisian historical heritage were selected: the "Saint-Maximin roche fine" (SM), the "Liais of Saint-Maximin" (LSM), and the "Chauvigny" (CH). All of these samples are marine limestones mainly composed of calcite (97%).

In detail, SM comes from the fine stone bench of Saint-Maximin quarry (Ouachée et Corpechot, Oise, France). This stone belongs to the Middle Lutetian (about 45 Ma ago, Cenozoic) and is formed during a sedimentation process occurring in warm and shallow water. Scarcely employed in the Roman Age (Thermes of Cluny, Paris), SM is essentially used since the nineteenth century thanks to the development of rail transportation. Nowadays, SM is often used for restoration works in elevated parts and cornices (e.g., Louvre Palace, Royal Palace, Invalides, Panthéon, and Versailles castle).

LSM limestone comes from the same quarry; it is also formed more recently (Upper Lutetian, about 43 Ma ago) than the SM. This stone possesses a wackestone structure and can be found in a layer thickness ranging from 30 to 50 cm (Merle 2008). Denser than the SM, LSM is generally considered as the nobler level of Lutetian limestone and is used and sculpted in vertical bed (e.g., Notre Dame Cathedral portal in Liais of Paris). Moreover, its hardness makes it an ideal stone to be used as steps for historical monument (e.g., Church of Notre Dame des Blancs Manteaux).

CH belongs to the Bathonien stage (around 165 Ma ago, Middle Jurassic period). This limestone shows a grainstone structure characteristic of a warm climate and a shallow (< 3 m) carbonate platform and a high energy paleo-environment, similar to the sedimentation occurring nowadays in the Bahamas. It has been used in Paris in sculpture (e.g.,

Trocadero column, bas relief of the façade of the Porte Dorée Palace), on structural or sculptured parts (e.g., Alexandre III Bridge), or in the elevated parts of monuments (e.g., Orsay Museum).

## Petrography and pore space characterization

The petrographic characterization of the limestone was performed on thin sections observed under a polarized light microscope (Leica Leitz Laborlux 12POLS) used in transmission mode and connected to a CCD camera managed by an image processing system (Histolab, Microvision®). The microfacies were identified using the carbonated stone classifications of Folk (1959) and Dunham (1962).

The pore space was observed on thin section of rock preliminary impregnated with two colored resins, according to the procedure described by Zinszner and Meynot (1982) and Pellerin and Zinszner (2007). Acting as a wet fluid, the red epoxy resin filled the free porosity of the stone sample by capillary imbibition at atmospheric pressure (under diphasic conditions). After polymerization of the red resin, the trapped porosity, non-accessible by water and occupied by air (non-wetting fluid), was filled manually with blue epoxy resin spreading on the cut surface.

## Porosity quantification and pore access radii distribution

The porosity was quantified by the measurements of two parameters: the water total porosity Nt (%) and the mercury porosity NHg (%). According to the AFNOR B10-615 standard procedure (2007), the samples were dried at 60 °C until they reached a stable mass ($m_d$). They were then degassed during 24 h in an airtight enclosure before being progressively saturated, from their bottom, with a degassed and deionized water under a dynamic vacuum. The total porosity (Nt) is given by the expression $Nt = [(m_1 - m_d) / (m_1 - m_2)] \times 100$, where $m_1$ is the mass of the sample totally saturated with a degassed and distilled water and $m_2$ is the mass of the underwater sample. NHg is obtained applying the Standard ASTM D4404-10 procedure (2010) by mercury-injection porosimetry. The mercury porosimetry determines the pore access radii ($R$) distribution in terms of mercury pressure-volume ($V$) injected inside the porous network. The distribution curve ($dV/d\log R$) is calculated from 200 μm (0.0037 MPa) to 0.0036 μm (206 MPa). The apparatus used is a Micromeritics AutoPore IV 9500 V1.09 porosimeter.

## Water transfer (capillarity and evaporation)

The water capillary imbibition is measured using the "classical" and the "environmental" approaches. The classical or "normative" approach follows the standard AFNOR B10-613 method (AFNOR 1999). In this case, cylindrical samples ($Ø \sim 4$ cm, $L \sim 5.5$ cm) are placed vertically, on a grid, in contact of a small layer of deionized water (5 mm) that fills the bottom of a closed chamber. The capillary suction provokes a water uptake of the samples which are regularly weighed.

The environmental one is a new and complementary approach, specially developed in order to make a characterization of samples submitted to realistic wet deposition event far from capillary rises. It consists in the direct measurement of the water uptake during the experiments performed in the CIME2 chamber. Samples (5 cm × 5 cm × 7 cm) are wrapped in a Teflon film with the exception of the front face (5 cm × 5 cm) which receives the spray simulating a driven rain or a driven drizzle event.

For the two approaches, according to Washburn's equations derived from Poiseuille's law and capillary pressure, the pore water volume (wetting phase) and consequently, the pore water mass is proportional to the square root of time. Usually, authors (David et al. 1993; Hammecker and Jeannette 1994) plot the mass increase relative to the contact surface area $\delta W/S$ (g cm$^{-2}$) to the square root of time. The capillary imbibition coefficient $A$ (g cm$^{-2}$ h$^{1/2}$) that expresses the mass increase rate by capillary imbibition corresponds to the slope of the first linear part of the curve of the mass increase versus the square root of time. The second part of the curve, with a lower slope, corresponds to the progressive invasion by water of the remaining macro-mesoporosity occupied by the air. The air diffuses through the water with slower kinetics according to the Fick's law.

The samples saturated by capillary water were then exposed to drying conditions. Here again, two ways are explored: the normative and the environmental. The normative approach consisted in enveloping the water-saturated stone cylinder in a Teflon film but leaving the summit face free. The sample was then submitted to a drying by exposition in a chamber where the relative humidity of 33% is controlled by a supersaturated solution of $MgCl_2$. Sample is regularly weighted and the evaporation curve expressed as the evolution of $\delta W/S$ (g cm$^{-2}$) versus time according to the Rousset-Tournier et al. (2003) and Turmel et al. (2014) protocol.

The environmental approach consists in the exposure of the sample in the CIME2 chamber where a dry air zero circulation simulates the wind conditions under which the stones exposed in Paris town can be submitted (see "CIME2 wet deposition chamber" section).

Generally, a classical evaporation curve includes three stages. During the first, the capillary water supply is sufficient to ensure a hydraulic continuity in the porous network to the surface submitted to evaporation (drying surface). The surface submitted to evaporation remains wet during all this stage of drying, while the water flow through the top surface is constant. During the second stage (intermediate stage), the water

flow decreases progressively; the water which leaves the top surface by evaporation is not totally replaced with water from inside the sample by capillary transfer, and then the top surface of the sample is partly wet. The third and last stage corresponds to another stage of drying with constant flow but much lower than the first one. The top surface of the sample is then dry and evaporation occurs from inside the stone to the drying surface by diffusion of water vapor within the porous network. Two parameters calculated at the end of the first stage (the critical hydric saturation Sc and the corresponding duration TSc) are characteristics of the sample submitted to a drying under controlled conditions.

## CIME2 wet deposition chamber

The CIME2 chamber has been designed to simulate the deposition of different precipitations. This chamber (Fig. 1a) is a transparent and waterproof Plexiglas box of 100 l (45-cm length, 53-cm height, and 48-cm depth). An inclined bottom-plane equipped with an exit point allows to carry away the excess water (condensation or runoff) during the wet deposition simulation. Several inlets and outlets allow the connection of a water supply or a drying system. For the simulation of rain event, a flat fan nozzle (jet angle 80°) supplied in water by a solenoid pump (flow of 45 to 100 ml $min^{-1}$) connected with a suction strainer immersed in deionized water at pH 6.1 delivers water droplets onto the sample (Fig. 1b). Sequential pulverizations are controlled by a timer. The simulation of mist or fog is generated by atomization of deionized water using a collision-type atomizer (AGK2000, Palas®), working at a pressure of 1.2 bar (Fig. 1c). To simulate evaporation or desorption, a drying system is used to decrease the relative humidity inside the chamber. The drying system (Fig. 1d) is a compressed air source which is dried (silica-gel column), decontaminated (active charcoal filter), and filtered (particles filter) to deliver a clean air (air zero).

During the experiment, the monitoring of environmental conditions (temperature and relative humidity) was performed using a Delta Ohm Hygrotransmitter HD9817T.3. The measurements of the sample's mass gain or loss during the humidification/drying cycles are provided by a sample holding device (Fig. 1e) placed underneath the balance base (Sartorius ED6202S-CW, weighing range 0.5–6200 g, accuracy 0.01 g) and suspending the sample at halfway up inside the chamber. Temperature, relative humidity, and mass values are monitored in real time using a Labview visualization system (Fig. 1f). The monitoring of the temporal evolution of the gain or loss of mass of the samples makes it possible to carry out petrophysical measurements in environmental conditions very close to those limestones of the built heritage of Paris town are exposed to.

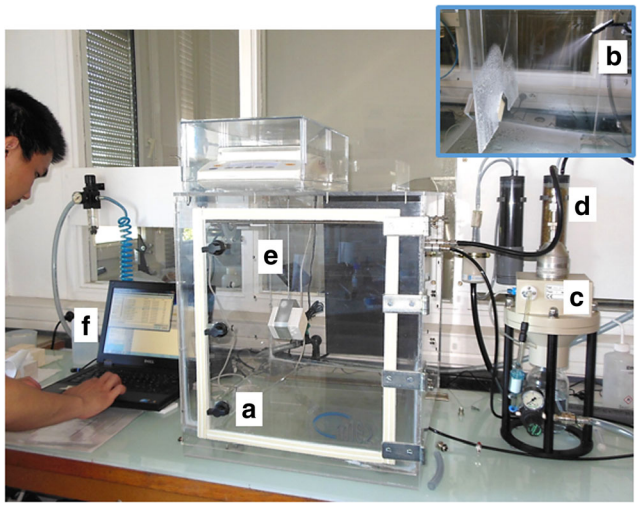


**Fig. 1** General view of the CIME2 alteration chamber dedicated to wet deposition simulation

## Rain and drizzle characterization

The spray used to simulate rain and drizzle events was characterized by a Phase Doppler Interferometer (PDI, Artium technologies Inc., LaVision). This PDI system performs a real-time and non-intrusive measurement of the individual droplets forming the spray (drop size ranging from 0.3 to 8000 μm). The geometrical position of the lasers ranges from − 200 mm to the left to + 200 mm to the right, with the center of the spray at position 0 mm. The laser measurements are performed at a 250-mm distance from the spray nozzle, which corresponds to the distance to the stone sample exposed inside CIME2. The droplets size and velocity distributions were determined every 10 mm, and from left to right within the spray. For the acquisition, the PMT gain (photomultiplier tube) ranged from 400 to 600 V, with a slit aperture varying between 200 and 1000 μm, a bin width of 1 to 2 μm, and a data acquisition frequency ranged of 10–560 Hz. The Sauter Mean Diameter (D32, μm) classically used to characterize a spray was used to study the size distribution of the droplets and to qualify the wet deposition (drizzle or rain).

## Mist characterization

To characterize the environment of CIME2 during the simulation of a mist event, a Mini Wide Range Aerosol Spectrometer Mini-WRAS 1371 (GRIMM®) was used to measure airborne particles generated by an atomizer ("CIME2 wet deposition chamber" section). By combining a stepping mode operated electrode with a Faraday cup electrometer and an optical aerosol spectrometer, the Mini-WRAS instrument gives an aerosol size distribution corresponding to electrical mobility diameter measurements (10 channels from 10 to 200 nm) and to the scattering light diameter measurements (31 channels from 0.2 to 35 μm). Every

minute, a pump working at a constant flow of 1.2 l $min^{-1}$ collects samples of the airborne particles, which are classified in 41 size channels. In parallel, the temperature and relative humidity are monitored within the chamber.

## Results and discussion

### Petrophysical characterization of the three limestones

#### Thin section observation

The Saint-Maximin "roche fine" (SM) limestone is a biosparite according to Folk's classification (1959) and has a grainstone structure according to Dunham's classification (1962). This rock is mainly composed of benthic foraminifer tests such as milioles (Fig. 2, SM). The petrographic and petrophysical characterization of SM has already been reported on similar samples in a previous paper (Saheb et al. 2016).

The Liais of Saint-Maximin (LSM) is a bioclastic limestone showing a packstone structure (Fig. 2, LSM). Foraminifer's tests mainly consist of milioles (larger than those of SM) and rare alveolines. Mollusca fragments are observed in places in the rock as well as some intraclasts and pellets. Angular detrital quartz grains are more abundant than in SM. These allochems are essentially bonded by micritic matrix bordered by a cement composed of microsparite crystals.

The free porosity is mainly placed at the borders of rounded or elongated macropores which can reach a length of several mm. Some free microporous zones are present in micrite grains (intraclasts, peloids, test lodges…). The trapped porosity, ubiquitous, is located in the center of the macropores, in the fossil chambers and between the sparite crystals of the cement.

The Chauvigny (CH) limestone is mainly made of isolated or composite ooliths (Fig. 2, CH). The edges of the ooliths are often underlined by a thin border of sparite crystals. Rare bioclasts (mollusk, corals) are locally present. The cement is mostly sparitic with some crystals that reach millimetric size.

The free porosity consists of intergranular macropores and isolated intragranular micropores placed in ooliths and micritized bioclasts. The trapped porosity is often placed in the middle of the large area of free porosity in large intergranular pore spaces and forms round zones of several hundred of micrometers. It occupied also some small zones (tens of micrometers) within bioclasts or sparite cement areas.

#### Porosity and pore access radii distribution

The quantification of the water porosity (Fig. 2) shows that SM has the highest porosity (~ 32%) followed by LSM (~ 27%) and CH (~ 16%). These percentages are coherent with mercury porosity measurements (Fig. 3). The pore access radii distribution (Fig. 3) is bimodal for SM (18 μm; 0.15 μm) and CH (85 μm; 0.2 μm). These two modes allow the filling of intergranular and intragranular free porosity organized in macro and micropores. However, for SM, the principal access radii is macroporous (18 μm). For CH, the two modes have

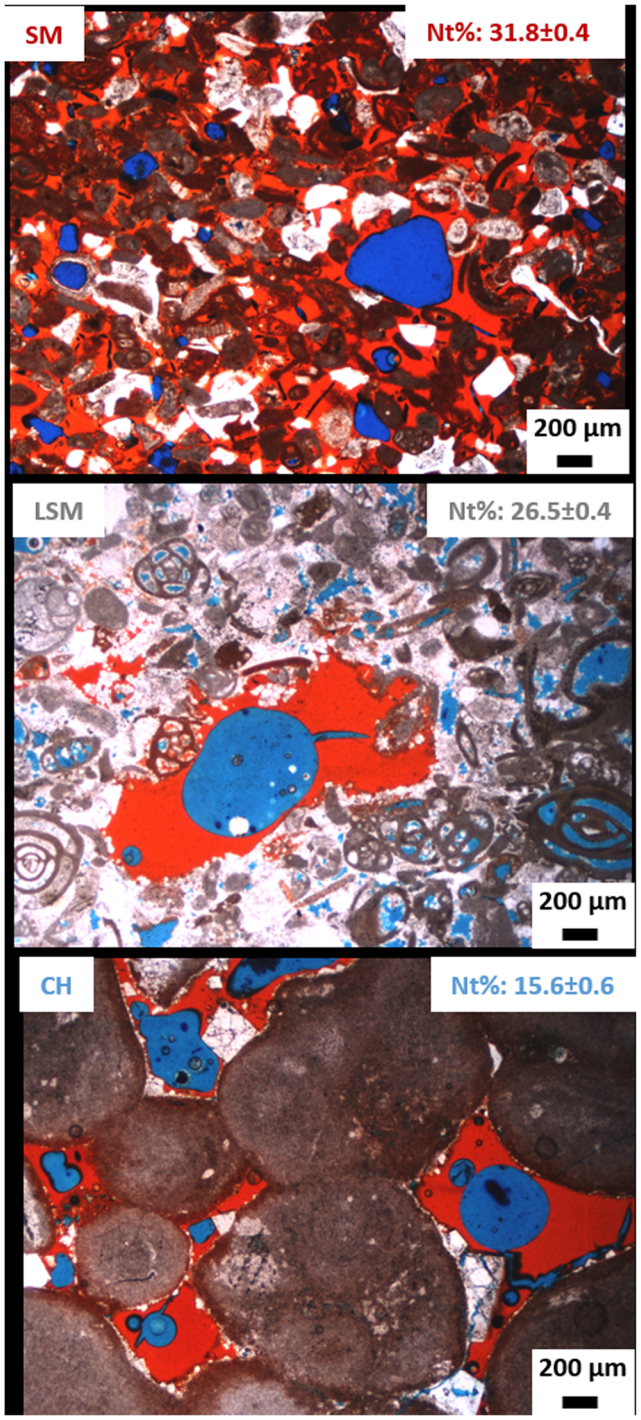


**Fig. 2** Thin sections of Saint-Maximin (SM), Liais of Saint-Maximin (LSM), and Chauvigny (CH) limestones embedded with twin colored resin showing the free (red) and the trapped (blue) porosity (polarized and non-analyzed light)

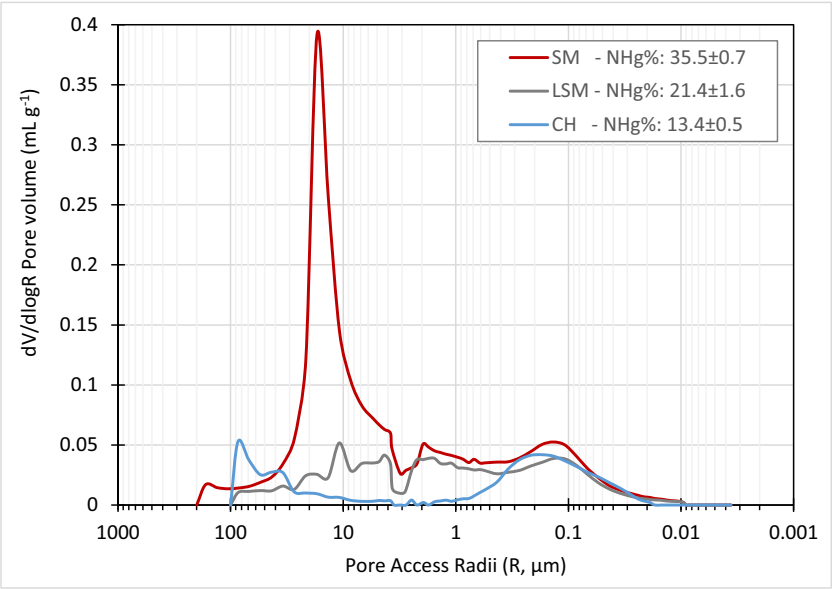


**Fig. 3** Pore access radii distribution of Saint-Maximin (SM), Liais of Saint-Maximin (LSM), and Chauvigny (CH) limestones by mercury porosimetry

the same ability of free porosity filling. On the contrary, LSM shows a very poorly sorted pore size distribution ranging from 100 to 0.02 µm. The filling of the LSM's free porosity (macro and micropores) is thus provided by any size of access radii.

### Normative capillary imbibition (AFNOR B10-613 1999)

The standardized capillary imbibition experiments (Fig. 4) show mass increase per unit of surface area versus square root of time curve organized into two linear phases. For all these three limestones, the linearity of these two phases and the coincidence between the arrival time of the capillary fringe at the top of the test sample ($\delta L$) and the filling time of the free porosity ($A$ slope) allows to consider unimodal their pore network, in which the distribution of the pores is quite homogeneous. The capillary imbibition coefficients ($A$) are on average $3.772 \pm 0.19$ g cm$^{-2}$ h$^{1/2}$ for SM, $0.525 \pm 0.16$ g cm$^{-2}$ h$^{1/2}$ for LSM, and $0.172 \pm 0.03$ g cm$^{-2}$ h$^{1/2}$ for CH, respectively. These coefficients are consistent with the order of the percentage of porosity measured by water and mercury injection. Moreover, initial values reflect the discrepancy in capillary water uptake with higher value for SM, then LSM, and finally CH.

### Normative evaporation (Rilem II5 norm, 1980)

The evaporation curves of the three limestones (Fig. 5) are organized into three typical stages: rapid desaturation with constant flow, desaturation with decreasing flow, and slow desaturation at constant flow. For the first phase of desaturation, the comparison of the coefficient shows differences in the flow. Indeed, the constant is similar for LSM ($-0.009 \pm 0.0004$ g cm$^{-2}$ h) and CH ($-0.009 \pm 0.0003$ g cm$^{-2}$ h) but the SM coefficient is slightly different with a value of $-0.007 \pm 0.0003$ g cm$^{-2}$ h, implying a slower desaturation for this stone. The critical water saturation values (Sc) expressed in percentage are respectively $28 \pm 6\%$ for SM, $38 \pm 3\%$ for LSM, and $39 \pm 1\%$ for CH. These percentages indicate that a major part of the evaporation occurs inside the three stone. The water saturation times (TSc) are $229 \pm 5$ h for the SM, $95 \pm 2$ h for the LSM, and $58 \pm 3$ h for CH. The complete desaturation is obtained after nearly 500 h for CH and 948 h for LSM. For SM, the complete desaturation time can require up to 5 months showing that in-depth evaporation takes a very long time for such stone.

## Characterization of the rain

Precipitations formed within the spray were analyzed by PDI. The scanning of the spray from its center towards its left and right external parts reveals that the particle diameters are in the 10–320-µm range (Fig. 6). At the center of the spray (0-mm position, black curve), the droplet number is relatively low (2300) and their diameter centered on $102 \pm 36$ µm. On the left side (dotted curves), in the strong part of the left jet found at position −120 mm (yellow), the number of counted droplets is much larger and the size distribution clearly bimodal. The main mode contains 13,415 droplets and is centered on a diameter of $114 \pm 31$ µm whereas the minor mode contains 2393 droplets with an average diameter of $193 \pm 23$ µm. On the right side (continuous curves), at position 90 mm (red) corresponding to another strong jet, the drop distribution is also found to be bimodal, with 19,796 drops in the main mode centered on $111 \pm 34$ µm and 8196 drops in the second mode centered on $187 \pm 28$ µm. In the most external left and right parts of the spray, the number of droplets decreases (1000 and 2600 drops,

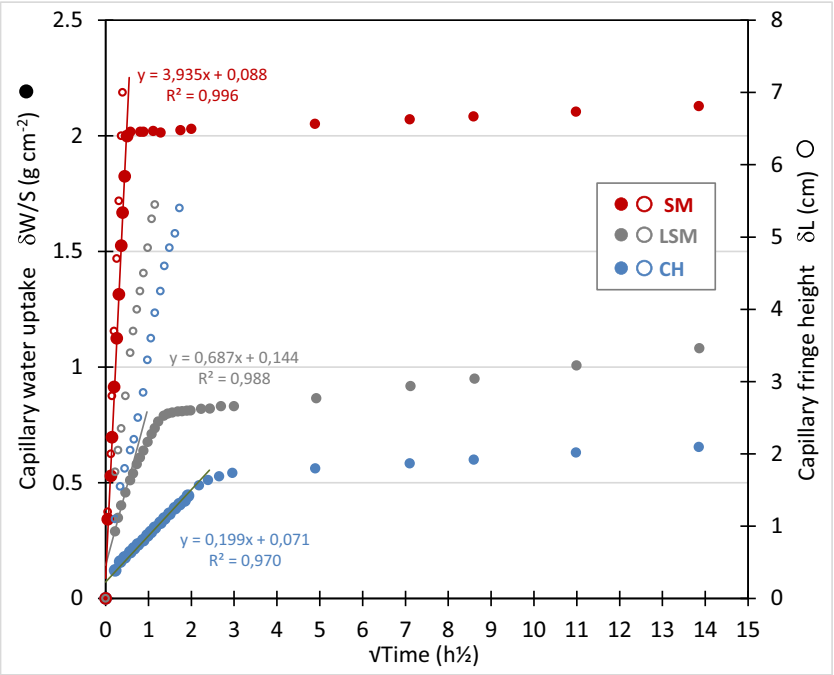


**Fig. 4** Examples of normative capillary imbibition curves of Saint-Maximin (SM), Liais of Saint-Maximin (LSM), and Chauvigny (CH) limestones

respectively) and tends to have a unimodal distribution centered on a larger diameter: 192 ± 19 μm for the position − 180 mm (black) and 184 ± 33 μm for the position 140 mm (green).

The velocity of the drops at different positions (left, center, right) has also been measured and found to range from 0 to 12 m $s^{-1}$ (Fig. 7). In the strongest parts of the spray, the distribution of the velocities contains two modes centered on 1.7 ± 0.5 and 3.7 ± 0.9 m $s^{-1}$ (for the – 120-mm position) and 2.0 ± 0.5 and 4.7 ± 1.9 m $s^{-1}$ (for the 90-mm position). Around the center of the spray (between position 0 and 60 mm), the velocity varies from 0.6 ± 2.2 to 0.7 ± 0.2 m $s^{-1}$. On the most external parts of the spray, the distribution of the velocity tends to become mono-modal but with the highest standard deviation: 1.5 ± 1.4 m $s^{-1}$ and 3.5 ± 1.8 m $s^{-1}$ at positions − 180 and 140 mm, respectively.

The classification of precipitations varies from one author to another and depends on the measurement process and the statistical analyses used. According to the MétéoFrance's

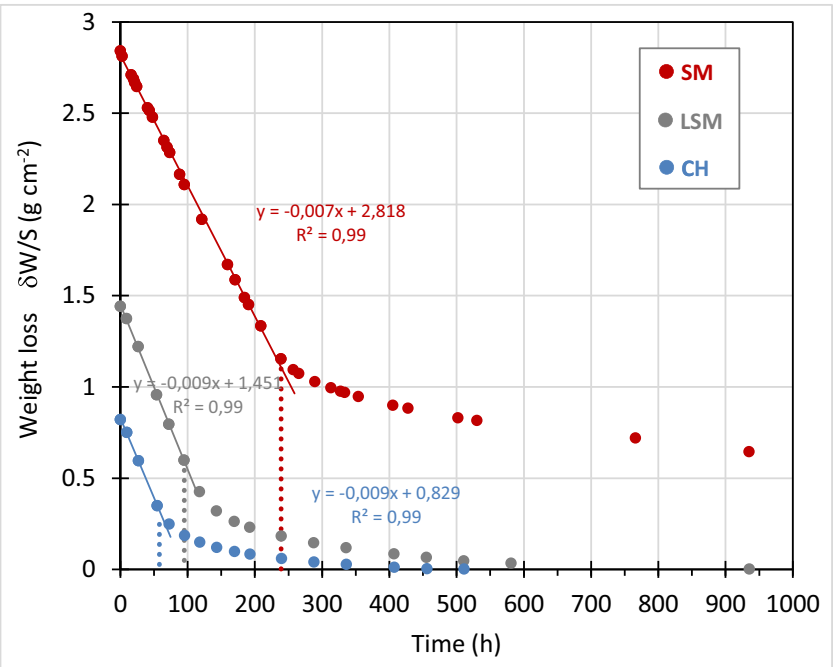


**Fig. 5** Examples of normative evaporation curves of Saint-Maximin (SM), Liais of Saint-Maximin (LSM), and Chauvigny (CH) limestones

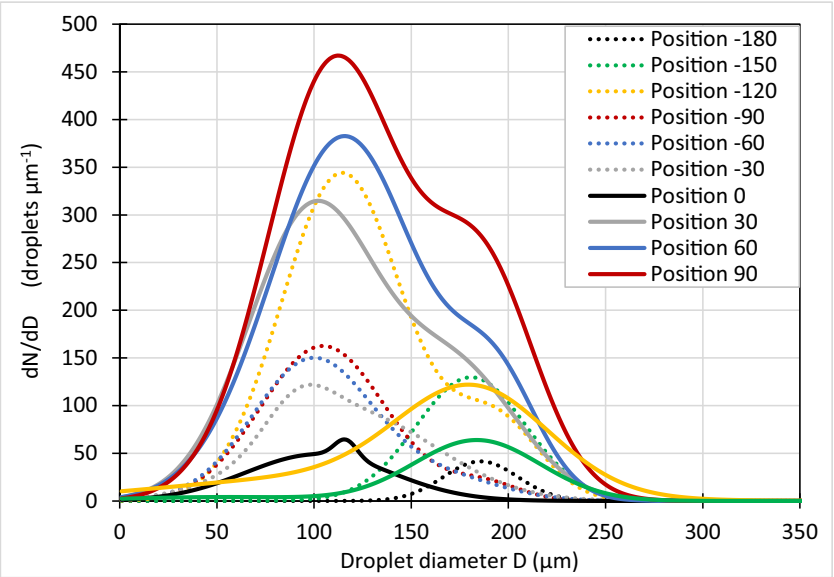


**Fig. 6** Size distribution of the rain and drizzle droplets produced by spraying inside the CIME2 chamber

glossary (http://www.meteofrance.fr/publications/glossaire), the size (diameter $D$) and the fall velocity ($v$) of the drops are the parameters usually used to discriminate precipitations such as drizzle or rain: droplets with $D > 500$ µm and $v > 1$ m s$^{-1}$ are classified as rain and those with $D < 500$ µm and $v < 1$ m s$^{-1}$ as drizzle.

Adopting these definitions, the spray used in the CIME2 chamber simulates drizzle and rain according to the fall velocity. In terms of size, droplets produced are too small for a typical rain but of good range for drizzle. Having in mind than rain event is polydispersed, we decided to qualify as "fine rain" the strongest parts of the spray (jets at positions − 120 and 90 mm). Conversely, the center and external parts of the spray will be chosen for the simulation of drizzle-dominated events. The orientation of the spray will determined the fine rain or mist simulation.

## Characterization of the mist

The recordings of the relative humidity (RH) show that the transition between dry mist (RH < 60%) and humid mist (RH > 60%) occurs after 17–20 min of atomization. The highest RH obtained in the chamber throughout the experiments was 97.3%. The Mini-WRAS was used to evaluate the

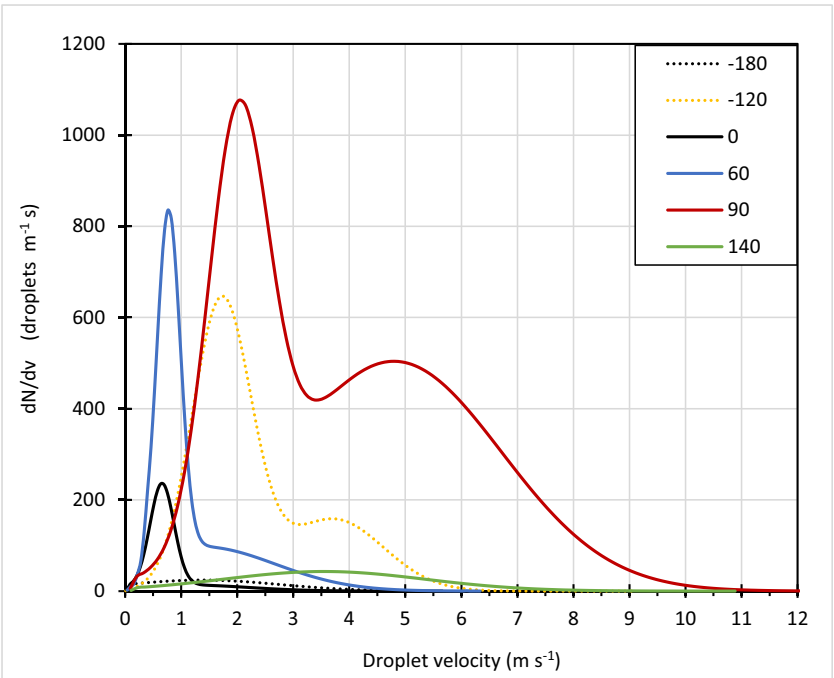


**Fig. 7** Fall velocity distribution of the rain and drizzle droplets generated by spraying inside the CIME2 chamber

size distribution of the mist droplets (Fig. 8). At $t_0$, the particle number concentration is very low (< $10^2$ particles per $cm^3$) and their sizes range between 10 and 150 nm due to the flushing of the CIME2 chamber by clean air. Between 0 and 25 min of atomization, the number of particles increases gradually up to $3.10^4$ particles per $cm^3$. The particle size distribution extends up to 1500 nm. After 25 min, the fine particles coagulate to form larger particles that reach 10 μm in diameter. Up to three size modes centered around 40, 200, and 3000 nm globally appear. The measurements were stopped at 25 min because of the formation of droplets on the filter head of the Mini-WRAS. The mist simulated in CIME2 is in good accordance with the reality. Indeed, in the field, the fog particle size distribution averages around 10 μm with larger drops diameters going up to 50 μm (Podzimek 1997; Hammer et al. 2014). These operating conditions thus appear as optimum to maintain a veil of fog all around the sample for the duration of the experiments.

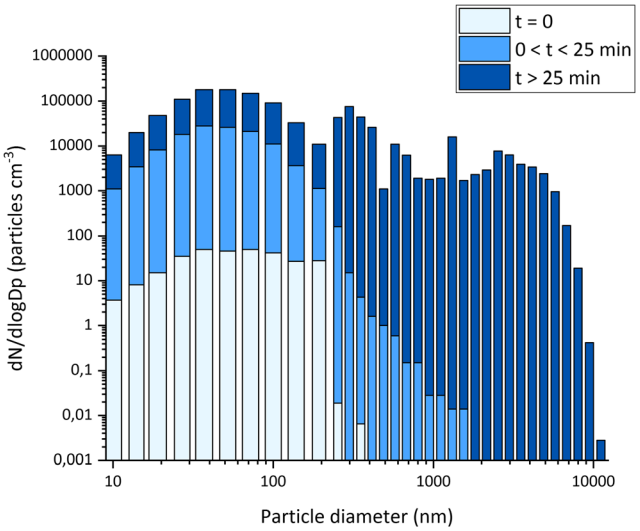


**Fig. 8** Size distribution of the mist particles produced by nebulization inside the CIME2 chamber

## CIME2 simulations of rain, drizzle, and drying event on limestones

### Rain and drizzle event

SM, LSM, and CH limestones were submitted to episodes of fine rain and drizzle produced in the CIME2 chamber. In order to simulate rainfall as a shower, the spray is oriented so that the maximum drop production hits the limestone. The duration of rain episodes is chosen with regard to the time of the real meteorological events. According to MétéoFrance's glossary, a rain shower has a short life span ranging from a few minutes to maximum 1 h time. The duration chosen for the rain experiment is 30 min (0.71 $h^{1/2}$) in order to have a time of imbibition that favors water transfer process change from liquid water transfer by capillarity to water vapor diffusion if permitted by the stone porous network.

For the drizzle, the nozzle is oriented towards the fallout of very soft and fine droplets. According to MétéoFrance's glossary, the drizzle never falls as a short rainfall but in a continuous way that lasts often several hours. In consequence, the duration retained for the drizzle event is 3 h (1.73 $h^{1/2}$), here also to ensure a significant capillary filling.

After a rainfall (continuous curves in Fig. 9), SM shows a linear increase in two stages, first a fast increasing linear stage ($A_{SM}$ 4.165 ± 0.21 g $cm^{-2}$ $h^{1/2}$), then a plateau phase registering a much slower increase which tends to stabilize at around 1.8 g $cm^{-2}$. The plateau is relatively close to the one reached in standardized measures (Fig. 4) performed on other similar samples. For LSM and CH limestones, after a short period (0.3 h) of non-linear evolution, the filling regime clearly follows a single linear stage ($A_{LSM}$ 0.663 ± 0.14 g $cm^{-2}$ $h^{1/2}$; $A_{CH}$ 0.399 ± 0.05 g $cm^{-2}$ $h^{1/2}$). The initial irregular stage occurs in the first time of the imbibition when the surface of the limestone is not yet entirely covered in water. Once the hydraulic continuity between the moistened surface and the subsurface is established, the water absorption follows a linear progression similar to standardized measurements (Fig. 4) but with a slower rate. The short duration of the rain events prevents a sufficient filling of the free porosity for LSM and CH. In other words, the second stage of filling of the macro-mesopores that needs air diffusion in water to the outside of the sample is reached only in the case of SM but not for LSM or CH. After 30 min of rainfall simulations, we can conclude that 100% of the porous network accessible by capillarity is reached for the SM limestone only. If compared to standardized measurements, about 70% of the pores are filled with water for LSM and about 55% for CH. By extrapolating, a duration of 1 and 1.5 h of rain would be necessary to fill free porosity of LSM and CH, respectively.

In the drizzle regime (dotted curves in Fig. 9), the filling of the porous network is slowed down for the three stones. On the scale of a 3-h event, an initial and irregular phase (0.8 ± 0.1 $h^{1/2}$ for SM, 0.4 ± 0.1 $h^{1/2}$ for LSM and CH) is followed by a linear mass gain. The capillary coefficients of the linear phase are weaker than those obtained after the rainfall event. SM linear phase (free porosity filling) stops after nearly 1.25 $h^{1/2}$ of event and the sample reaches the plateau phase of filling the porous network by diffusion. The plateau phase is observed at the same level than those of standardized measurements (Fig. 4) and rain event (Fig. 9). LSM and CH reach an important level of filling despite a capillary coefficient lower that under rain regime due to the longtime and the continuous alimentation of water by drizzle. However, the phase of porous network filling by diffusion is not achieved for LSM and CH. After 3 h of drizzle, we can conclude that 100% of the porous network accessible by capillarity is reached for the SM

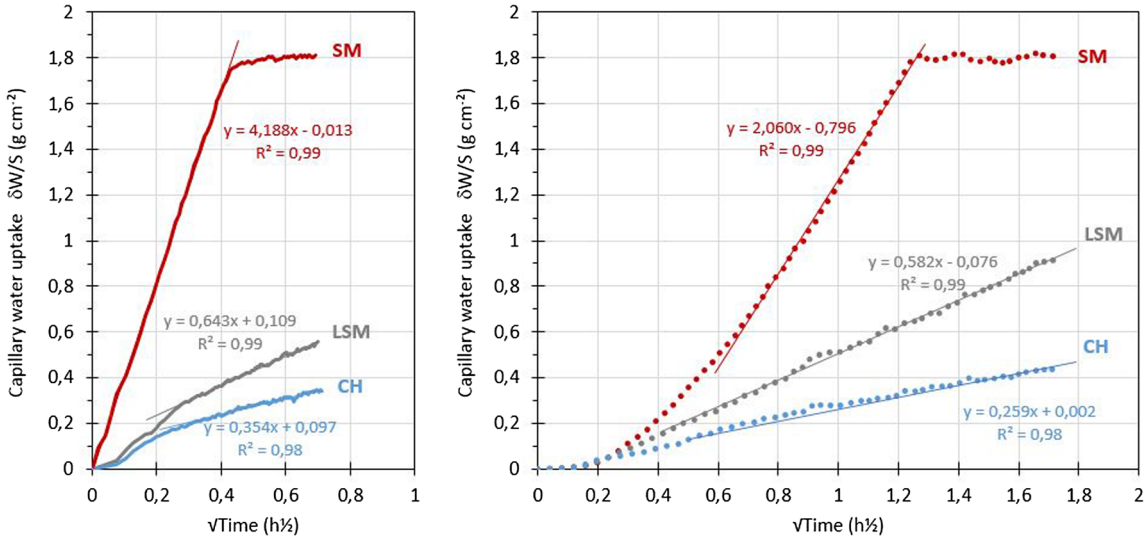


**Fig. 9** Examples of environmental capillary imbibition curves of Saint-Maximin (SM), Liais of Saint-Maximin (LSM), and Chauvigny (CH) limestones submitted to 30 min of rainfall (continuous curves) and 3 h of drizzle (dotted curves) inside the CIME2 chamber

limestone only. For LSM and CH, the free porosity filling is not completed.

### Comparison between standard (0°) and realistic evaporation under air flow (1°–2°Beaufort)

Air velocity measurements using a hot wire anemometer were performed in the CIME2 chamber during air zero drying. At the sample level, the air velocity measured oscillates between 0.485 and 2.1 m $s^{-1}$. These values correspond to 1° (light air) to 2° (light breeze) on the Beaufort's scale. Statistics carried out between 1971 and 2000 (MétéoFrance collectif) show that the wind speed in Paris is mainly ranged between 1.5 and 4.5 m $s^{-1}$ (69.4%) and between 0 and 1.5 m $s^{-1}$ (10.9%). The drying regime produced in CIME2 is therefore very realistic and reproduces rather well the Paris environmental conditions.

Whatever the wet deposit (rainfall or drizzle), the evaporation curves obtained during the realistic drying (Fig. 10) start with a short non-linear phase that can be attributed to the runoff of the last droplets present on the limestone surfaces. After this stage, the three limestones show a mass loss which reproduces the three steps described on the normalized curves (Fig. 5). The drying curves obtained after the rainfall event (Fig. 10, linear curves) show a linear phase of desaturation with constant flow ending after 9 ± 0.25 h for SM, 3 ± 0.2 h for LSM, and 1 ± 0.1 h for CH; a desaturation phase at decreasing flow; and a last phase of desaturation at constant flow that starts at 16 ± 0.25 h for SM, 8 ± 0.2 h for LSM, and 5 ± 0.1 h for CH.

After drizzle (Fig. 10, dotted curves), SM shows an evaporation curve, which is overlaid (same desaturation coefficient) on that obtained after rain. This is linked with the total filling of the SM capillary porous network during the two simulated events. For LSM and CH, the time of the first phase of evaporation at constant flow is longer for drizzle than for rain. This is also linked with the higher amount of water that soaked LSM and CH during the drizzle. It requires 4 ± 0.2 h for LSM and 3 ± 0.1 h for CH for the evaporation that occurs towards the limestone surface. The beginning of the in-depth evaporation phase occurs also later, 14 h ± 0.1 h for LSM and 10 ± 0.1 h for CH. In comparison with the normalized data (Fig. 5), the evaporation time under realistic conditions is considerably shortened through air circulation (factor 25).

## Simulation of mist events on limestones

Fog (mist) events were reproduced in the CIME2 chamber to measure the amount of water adsorbed and identify, if possible, a capillary condensation phase occurrence. Two mist events were firstly simulated in order to create an autumnal morning (6 h) and then a winter foggy day (20 h) in Paris according to local meteorological statistics (MétéoFrance collectif 1971). After 6 and 20 h (Fig. 11), as expected, the mass uptake regularly increases but stays weak for the three limestones. This low amount of water fixation corresponds theoretically to the filling of sites whose radius is less than 0.1 μm according to Kelvin's law. No saturation phase is reached whatever the limestone. Fog test lasting 7 days was then conducted on the three limestones. This duration corresponds to an exceptional fog event that can occur in winter in Paris. During this longer period, LSM and CH show a similar and gradual increase in water fixation. It is interesting to notice for SM a clear increase of water fixation after 48 ± 1 h followed by a weaker increase after 96 ± 1 h, which announces a phase of saturation. The amount of water fixed by SM is in the same range of order than that measured after 0.08 h during the capillary test. In that case, we can consider that a

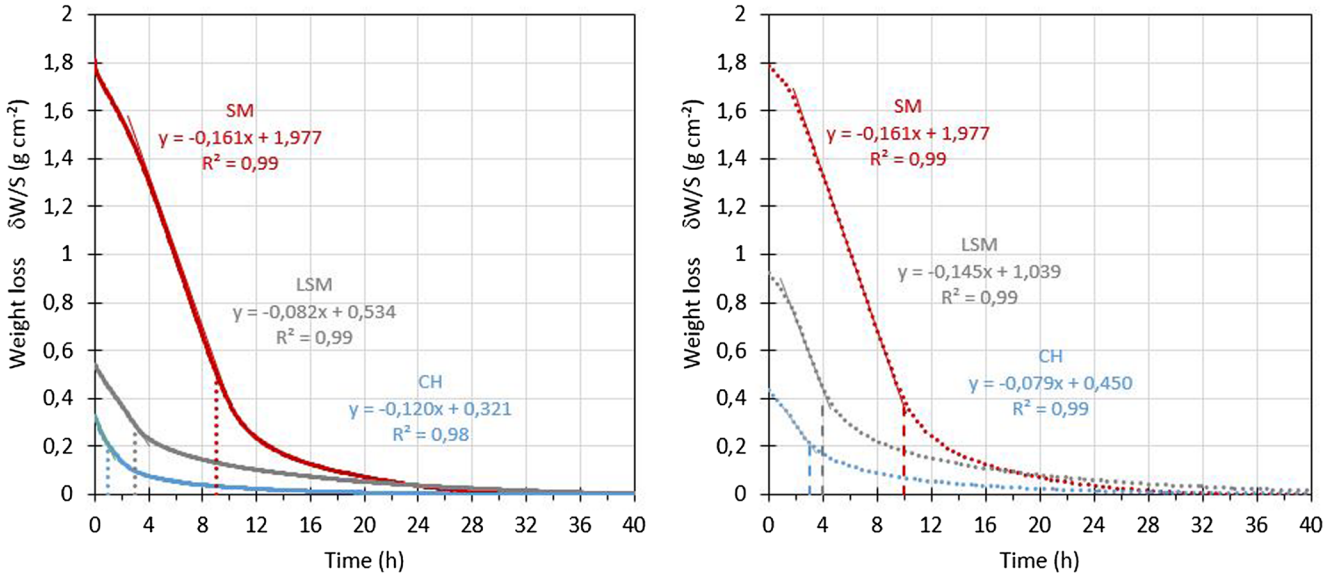


**Fig. 10** Examples of environmental evaporation curves of Saint-Maximin (SM), Liais of Saint-Maximin (LSM), and Chauvigny (CH) limestones under 1°–2° Beaufort air circulation after 30 min of rainfall (continuous curves) and 3 h of drizzle (dotted curves) inside the CIME2 chamber

phenomenon of capillary condensation and a surface condensation on the surface roughness have probably occurred on SM. However, the RH (limited to 97.6 ± 0.5%) does not permit a more important filling of the porosity.

## Concluding remarks

The CIME2 experimental chamber has been specifically developed to simulate wet deposition on cultural heritage materials. Three limestones typically used in Paris monuments have been tested. The operative conditions have been optimized to reproduce rain-dominant, drizzle-dominant, and mist deposition on limestone samples. Moreover, the wind conditions of Paris have been simulated to quantify their influence of the kinetics on limestone drying. In parallel with wet deposition or drying, a real-time measurement of limestone mass gain or mass loss was achieved. The data acquired allow documenting the limestones water imbibition and evaporation curves, in a way similar to that of the traditional AFNOR & RILEM petrophysical standards but revisited and improved in the sense that they are dimensioned to be much closer to real environmental conditions of Paris. The comparison of the standard method with the new environmental one

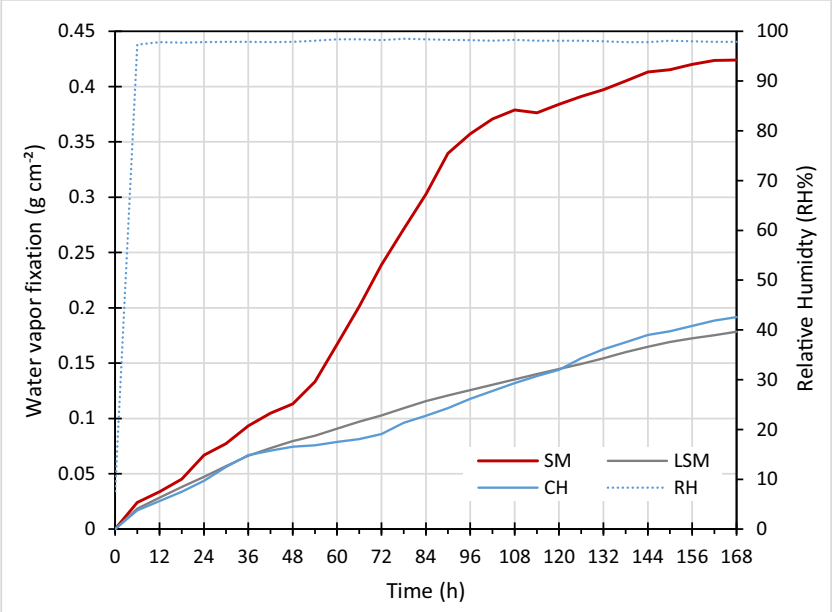


**Fig. 11** Examples of experimental curve of water fixation on Saint-Maximin (SM), Liais of Saint-Maximin (LSM), and Chauvigny (CH) limestones under mist regime inside the CIME2 chamber

shows that the former systematically overestimates the amount of absorbable water by capillary imbibition but underestimates the kinetics of the evaporation. In addition, the wet deposition simulation performed in CIME2 clearly evidences a porous network unsaturation for microporous limestones of Chauvigny and Liais of Saint-Maximin. The unsaturation state is also favored by a more rapid drying in real condition for the three limestones.

In the current context of global change, the climate models predict that the frequency of extreme rain and wind events will increase. This may influence the degree of limestone unsaturation. An interesting way of supplementing the results of this study could be in documenting better the site of water migration and reactivity during this unsaturation phase using isotope tracers such as $^{2}H_2O$ and $^{18}O$. This would allow a better individualization of the zones of risk (erosion), passivation, or resumption of alteration in zones affected by water transfer. The CIME2 chamber will be particularly well adapted to explore this future axis of research, not only on limestones but also on other materials of the cultural heritage. In the future, the modeling of weathering phenomena will have to be improved in order to take into account this particularity and the resulting additional complexity of unsaturation, which is currently often disregarded in the geochemical models.

**Acknowledgments** This work was supported by the DIM R2DS French Regional Program (2013–2017) and the French National Research Agency (ANR JCJC GLAM Project (2014–2018). The authors thank J. Vatteville from LaVision for the PDI measurements.

## References

AFNOR (1999) AFNOR B10-613, Méthodes d'essai pour pierres naturelles - Détermination du coefficient d'absorption d'eau par capillarité. Standard NF EN 1925. Association Française de Normalisation (AFNOR), Paris

AFNOR (2007) AFNOR B10-615, Méthodes d'essai des pierres naturelles - Détermination des masses volumiques réelle et apparente et des porosités ouverte et totale. Standard NF EN 1936. Association Française de Normalisation (AFNOR), Paris

ASTM D4404-10 (2010) Standard test method for determination of pore volume and pore volume distribution of soil and rock by mercury intrusion porosimetry. pp. 7

Ausset P, Crovisier JL, Del Monte M, Furlan V, Girardet F, Hammecker C, Jeannette D, Lefèvre R (1996) Experimental study of limestone and sandstone sulphation in polluted realistic conditions: the Lausanne atmospheric simulation chamber (LASC). Atmos Environ 30:3197–3207

Bernardi E, Chiavari C, Lenza B, Martini C, Morselli L, Ospitali F, Robbiola L (2009) The atmospheric corrosion of quaternary bronzes: the leaching action of acid rain. Corros Sci 51:159–170

Beysens D, Mongruel A, Acker K (2017) Urban dew and rain in Paris, France: occurrence and physico-chemical characteristics. Atmos Res 189:152–161

Bonazza A, Sabbioni C (2016) Composition and chemistry of crusts on stone. In: Brimblecombe P (ed) Air pollution reviews no. 5. Urban pollution and changes to materials and building surfaces. Imperial College Press, London, pp 103–123

Bonazza A, Messina P, Sabbioni C, Grossi CM, Brimblecombe P (2009) Mapping the impact of climate change on surface recession of carbonate buildings in Europe. Sci Total Environ 407(6):2039–2050

Buhmann D, Dreybrodt W (1985) The kinetics of calcite dissolution and precipitation in geologically relevant situations of karst areas. Chem Geol 48:189–211

Camuffo D (2016) Weathering of building materials. In: Brimblecombe P (ed) Air pollution reviews no. 5. Urban pollution and changes to materials and building surfaces. Imperial College Press, London, pp 19–64

Chabas A, Fouqueau A, Attoui M, Alfaro S, Petitmangin A, Bouilloux A, Saheb M, Coman A, Lombardo T, Grand N, Zapf P, Berardo R, Duranton M, Durand-Jolibois R, Jerome M, Pangui E, Correia JJ, Guillot I, Nowak S (2015) Characterization of CIME, an experimental chamber for simulating interactions between materials of the cultural heritage and the environment. Environ Sci Pollut Res 22: 19170–19183

Chiavari C, Bernardi E, Martini C, Passarini F, Ospitali F, Robbiola L (2010) The atmospheric corrosion of quaternary bronzes: the action of stagnant rain water. Corros Sci 52:3002–3010

David C, Darot M, Jeannette D (1993) Pore structures and transport properties of sandstone. Transp Porous Media 11:161–177

Dewanckele J, De Kock T, Fronteau G, Derluyn H, Vontobel P, Dierick M, Van Hoorebeke L et al (2014) Neutron radiography and X-ray computed tomography for quantifying weathering and water uptake processes inside porous limestone used as building material. Mater Charact 88:86–99

Dunham RJ (1962) Classification of carbonate rocks according to depositional texture. In: Ham, W. E. (ed.) Classification of carbonate rocks. American Association of Petroleum Geologists, Memoirs, 1:108–121

Folk RL (1959) Practical petrographical classification of limestones. Am Assoc Pet Geol Bull 43:1–38

Franzoni E, Sassoni E (2011) Correlation between microstructural characteristics and weight loss of natural stones exposed to simulated acid rain. Sci Total Environ 412-413:278–285

Fripiat J, Chaussidon J, Jelli A (1971) Chimie physique des phénomènes de surfaces. Application aux oxydes et aux silicates. Edition Masson & Cie 387pp

Hammecker C, Jeannette D (1994) Modelling the capillary imbibition kinetics in sedimentary rocks: role of petrographical features. Transp Porous Media 17:285–303

Hammer E, Gysel M, Roberts GC, Elias T, Hofer J, Hoyle CR, Bukowiecki N, Dupont JC, Burnet F, Baltensperger U, Weingartner E (2014) Size-dependent particle activation properties in fog during the ParisFog 2012/13 field campaign. Atmos Chem Phys 14:10517–10533

Icomos (2008) Illustrated glossary on stone deterioration patterns ICOMOS International Scientific Committee for Stone (ISCS). 86 pages

Inkpen RJ, Viles HA, Moses C, Baily B, Collier P, Trudgill ST, Cooke RU (2012) Thirty years of erosion and declining atmospheric pollution at St Paul's Cathedral, London. Atmos Environ 62:521–529

Le Moullec A, Mezdour A (2011) La qualité des eaux de pluie : acidité en baisse mais pas de progrès pour les dépôts d'azote. http://www.developpement-durable.gouv.fr/IMG/pdf/LPS88.pdf

Lefèvre RA, Ionescu A, Desplat J, Kounkou-Arnaud R, Perrussel O, Languille B (2016) Quantification and mapping of the impact of the recent air pollution abatement on limestone and window glass in Paris. Environ Earth Sci 75:1359

Livingston RA (1992) Graphical methods for examining the effects of acid rain and sulphur dioxide on carbonate stones. Proceedings of the 7th International Congress on Deterioration and Conservation of

Stone, Lisbon, 375-386. In: J. Delgado Rodrigues, F. Henriques & F.Telmo Jeremias (eds)

Livingston RA (2016) Acid rain attack on outdoor sculpture in perspective. Atmos Environ 146:332–345

Merle D (2008) Stratotype Lutétien. Muséum National d'Histoire Naturelle, Paris; Edition Biotope, Mèze; BRGM, Orléans, 288p

Météofrance collectif (1971-2000) Statistiques climatiques de la France. 287p. http://www.meteofrance.fr/publications/nos-collections/climat/statistiques-climatiques-de-la-france-19712000

Pellerin FM, Zinszner B (2007) A geoscientist's guide to petrophysics. IFP publication. Editions Technip

Plummer LN, Wigley TM (1976) The dissolution of calcite in $CO_2$-saturated solutions at 25°C and 1 atmosphere total pressure. Geochim Cosmochim Acta 40:191–202

Podzimec J (1997) Droplet concentration and size distribution in haze and fog. Stud Geophys Geod 41(3):277–296

Rousset B (2001) Transferts par capillarité et évaporation dans des roches – rôle des structures de porosité. Thèse de l'Université Louis Pasteur – Strasbourg 1. 220 pp.

Rousset-Tournier B, Mazerolle F, Geraud Y, Jeannette D (2003) Rock drying test monitored by x-ray computed tomography—the effect of saturation methods on drying behavior. In: Mees F, Swenner R, Van Geet M, Jacobs (eds) Application of X-ray computed tomography in the geosciences, vol 215. Geological Society, London, Special Publication, pp 117–125

Sabbioni C (2003) Mechanisms of air pollution damage to stone. In: Brimblecombe P (ed) Air pollution reviews. The effects of air pollution on the built environment. Imperial College Press, London, pp 63–106

Saheb M, Chabas A, Mertz JD, Colas E, Rozenbaum O, Sizun JP, Nowak S, Gentaz L, Verney-Carron A (2016) Weathering of limestone after several decades in an urban environment. Corros Sci 111:742–752

Smith BJ, Viles HA (2006) Rapid, catastrophic decay of building limestones: thoughts on causes, effects and consequences. International Conference on Heritage, Weathering and Conservation Location, 1, 191–197. Edited by: Fort R, Alvarez De Buergo M, Gomez Heras M et al. Madrid. Spain

Steiger M (2016) Air pollution damage to stone. In: Brimblecombe P (ed) Air pollution reviews no. 5. Urban pollution and changes to materials and building surfaces. Imperial College Press, London, pp 65–101

Tétreault J, Dupont AL, Bégin P, Paris S (2013) The impact of volatile compounds released by paper on cellulose degradation in ambient hygrothermal conditions. Polym Degrad Stab 98:1827–1837

Turmel A, Fronteau G, Thomachot-Schneider C, Moreau C, Chalumeau L, Barbin V (2014) Stone uses in Reims Cathedral: provenance, physical properties and restoration phases. In: Cassar J, Winter MG, Marker BR, NRG W, Entwisle DC, Bromhead EN, JWN S (eds) Stone in historic buildings: characterization and performance, vol 391. Geological Society, London, Special Publication, pp 17–30

Unterwurzacher M, Mirwald P (2008) Initial stages of carbonate weathering: climate chamber studies under realistic pollution conditions. Environ Geol 56:507–519

Zinszner B, Meynot C (1982) Visualisation des propriétés capillaires des roches réservoirs. Rev Inst Fr Pétrole 37:337–361